PROCEEDINGS OF SCIENCE

Commissioning, operation and performance of the CMS Silicon Strip Tracker detector

Stefano Mersi* **for the CMS Tracker Collaboration**
CERN
E-mail: stefano.mersi@cern.ch

The CMS Silicon Strip Tracker is a complex device, with about 15000 sensitive modules it is the largest Silicon tracker ever built. After a major intervention on its cooling system it was re-commissioned in summer 2009 and joined the all-CMS cosmic data taking with the nominal 4T field. This article shortly reviews the architecture of this detector, gives some result of the 2009 commissioning and shows the latest performance qualifications.

VERTEX 2009 (18th workshop) - VERTEX 2009
September 13 - 18 2009
Veluwe, the Netherlands

*Speaker.

PoS(VERTEX 2009)004

1. Description

The Silicon Strip Tracker (SST) is the tracking detector of the CMS experiment at LHC [1]. It comprises four sub-detectors: Inner Barrel (TIB), Inner Disks (TID), Outer Barrel (TOB) and End-Caps (TECs) and occupies a cylindrical volume 5.4 m long, with a diameter of 2.4 m around the interaction point. The detector is instrumented with 15 148 modules for a total active area of 198 m^2 and 9 316 352 channels with full optical analog readout. The chosen silicon sensors are a p-on-n strip with substrate thicknesses of 320 μm and 500 μm [2]. The strip length varies from 8.5 cm to 20.18 cm (obtained by combining two sensors per module) and the strip varies from 80 μm and 180 μm. Special *stereo modules* with a *stereo angle* of 100 mrad are used to build *double-sided* detectors providing 3D hits.

Construction of the SST was completed in 2007 and it was installed within CMS during 2008. The system underwent its first commissioning and first round of data taking with the other CMS sub-detectors during summer 2008. The first operation of the full SST in a 3.8 T magnetic field took place during October-November 2008, in an exercise known as Cosmic Run at Four Tesla (CRAFT 2008) [3]. The SST underwent a major cooling plant refurbishment in winter-spring 2009 and was finally re-commissioned in summer 2009 in time to participate to the CRAFT 2009 exercise.

In this paper the result of the 2009 commissioning are reported, together with the latest available performance measurements from CRAFT 2008 and CRAFT 2009.

2. Control and readout systems

The major components of the SST readout system [1] are: 15 148 front-end printed boards that host 72 784 APV25 [4] readout chips, an analogue optical link system comprising 36 392 individual fibers [5], and 440 off-detector analogue receiver boards, known as Front-End Drivers (FED) [6]. The SST control system [7] is driven by 46 off-detector digital transceiver boards, known as Front-End Controllers (FEC) [8]. The FECs distribute the LHC clock, triggers and control signals to the front-end detector modules via Communication and Control Units (CCU) [9], which are arranged on 368 token rings (*control rings*).

The APV25 readout chip samples, amplifies, buffers, and processes signals from 128 detector channels at a frequency of 40 MHz. The APV25 chip uses pre-amplifier and shaper stages to produce a CR-RC pulse shape with a relatively slow rise-time of 50 ns in an operating mode known as *peak*. An alternative mode, *deconvolution*, performs additional signal processing to constrain the signal to a single bunch crossing [10] at the expense of a reduced signal-to-noise ratio (Fig. 1). Deconvolution is expected to be the standard mode of operation.

On receipt of a Level-1 trigger, pulse height and bunch-crossing information from the APV25 chips are converted to optical analogue signals through lasers driven by dedicated Linear Laser Drivers (LLD) chips [11]. Data are transmitted via optical links to the off-detector FED boards. The FEDs digitize, compress, and format the pulse height data from up to 96 pairs of APV25 chips, before forwarding the resulting event fragments to the SST local data acquisition via VME readout or to the CMS data acquisition systems [12] via a dedicated S-Link bus.
The APV25 also produce a periodic *tick mark* calibration signal every 70 clock cycles.

3. Commissioning

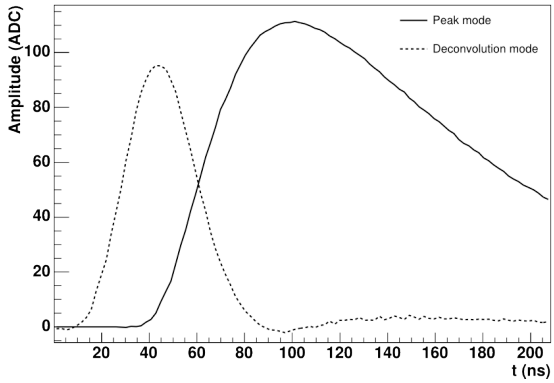

Figure 1: An example of the CR-RC pulse shape of a single APV25 chip, in Peak and Deconvolution mode.

In order to bring the SST in operational state a number of parameters must be set, both in the detector devices and in the readout electronics. Tuning these parameters is commonly referred to as *commissioning*.

The SST was commissioned for the first time in June-July 2008 and later included in the CRAFT 2008 data taking. The interruption of LHC operations in late 2008 allowed to perform a complete refurbishment of the two cooling plants serving the tracker in order to increase stability and to reduce cooling fluid leak observed in 2008 in some of the 180 cooling lines.

This intervention also allowed to safely decrease the operational temperature of the cooling plant from 11 °C to 4 °C. Given the change of environmental conditions a new detector commissioning was necessary to optimize the detector performance. During this commissioning the SST was tuned for the first time to operate in the nominal deconvolution mode. The following sections describe the commissioning procedures and results from 2009.

3.1 Front-end synchronization

Relative synchronization involves adjusting the phase of the LHC clock delivered to the front-end by varying the clock phase using a Phase Locked Loop (PLL) chip [13] hosted by each detector module so that the sampling times of all APV25 chips in the system are synchronous. Additionally, the signal sampling time of the FED Analogue/Digital Converters (ADC) is appropriately adjusted. This procedure accounts for differences in signal propagation time in the control system due to differing cable lengths and uses the APV25 tick mark as a timing reference and dedicated fiber length measurements [14].

This synchronization procedure is important because the signal amplitude is attenuated by as much as 4% per nanosecond mis-synchronization due to the narrow pulse shape in deconvolution mode. With this procedure the timing spread is reduced to an RMS of 0.7 ns.

3.2 Readout calibration

During this procedure the gain register settings of the LLD chip are tuned for individual fibers. The amplitude of the APV25 tick mark is used to measure the gain of each readout channel and choose the appropriate gain setting out of the four available, to optimize the use of the FED ADCs. Additionally a software calibration is obtained using the nominal correspondence of a tick mark to a charge deposit of 175 000 e^-. The estimated systematic uncertainty is 5%, attributable to the sensitivity of the tick mark amplitude to variations in the LV power supply and environmental temperature [15].

This is the calibration provided by the commissioning on top of which an additional calibration is computed off-line measuring the particle signal.

3.3 Tuning of the APV25 front-end amplifier pulse shape

The shape of the CR-RC pulse from the APV25 pre-amplifier and shaper stages is dependent on the input capacitance, which depends on the sensor geometry and evolves with total radiation dose. Non-uniformities in the fabrication process and environmental conditions result in a spread in the pulse shape parameters for a given input capacitance of 10% to 15%, for the non-irradiated detectors. This issue is important for performance in deconvolution mode, which is sensitive to the CR-RC pulse shape. The calibration pulse was analyzed for a wide range of parameters, and the latter were tuned to obtain an optimal pulse shape (rise time of 50 ns and 36% of the maximum signal amplitude 125 ns later).

3.4 Calibration of the detector channel pedestals and noise

The mean level of the pedestals for the 128 channels of a given APV25 chip, known as the *baseline* level, can be adjusted to optimize the signal linearity and the use of the available dynamic range of the APV25. The baseline level for each APV25 chip is adjusted to sit at approximately one third of the dynamic range (with a typical variance of 3%).

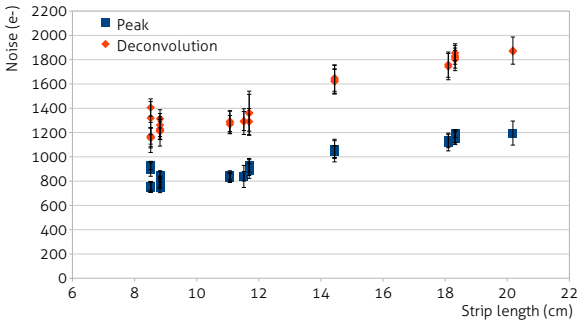

Figure 2: Average noise as a function of the strip length. Error bars represent the average APV noise variance.

The pedestal and noise constants for each individual detector channel must be measured, as these values are used by the zero-suppression algorithms implemented in the FEDs. Pedestals and noise are both measured using a random, low frequency trigger ($\sim$10 Hz) in the absence of signal. Pedestals are first calculated as the mean of the raw data in each detector channel from a large event sample. They are subsequently subtracted from the raw data values for each event. Common mode offsets are evaluated for each APV25 chip per event by calculating the median of these pedestal-subtracted data. The median value is then subtracted from each channel. The noise for each detector channel is then defined to be the standard deviation of the residual data levels, which can be individually calibrated using their tick mark measurements, as described above.

Modules with different sensor geometries are studied separately to account for the different strip lengths and layouts that affect the input capacitance. The mean normalized noise measured for the different sensor geometries are summarized in Figure 2. From a straight line fit to to the noise the following parameters are extracted:

$$\text{noise}_{\text{PEAK}} = (445 \pm 30)\text{e}^- + l \times (38 \pm 2)\text{e}^-/\text{cm}$$

$$\text{noise}_{\text{DECO}} = (646 \pm 50)\text{e}^- + l \times (64 \pm 4)\text{e}^-/\text{cm}$$

with l average strip length for a given geometry. The peak mode measurement is compatible with the one performed during 2008 commissioning [16]. The noise in deconvolution mode is uniformly higher by a factor 1.54 ± 0.03, similar to the estimation of 1.6 stated in the APV25 specifications.

3.5 Absolute synchronization to an external trigger

The last two commissioning procedures concern the synchronization of all modules in the SST with the Level-1 trigger of CMS. This was done using a dedicated trigger provided by the Muon Drift Tube sub-detector [17]. The procedure requires track reconstruction and the analysis was performed off-line [18]. Absolute synchronization accounts for both the delays introduced by the hardware configuration and the effects due to the time-of-flight of particles.

The first of the two procedures is a coarse scan in time, in steps of 25 ns, by adjusting the latency between the trigger arrival and the sampling time of the APV25 chip. The mean signal of the channel with the largest signal amplitude (*leading strip*) in clusters associated to reconstructed tracks was extracted as a function of the latency. The signal magnitude was corrected for the track path length through the active sensor volume, inferred from the track angle. The overall delay measured was then applied to all the sub-detectors, which were already synchronous, as expected (Figure 3 (left)).

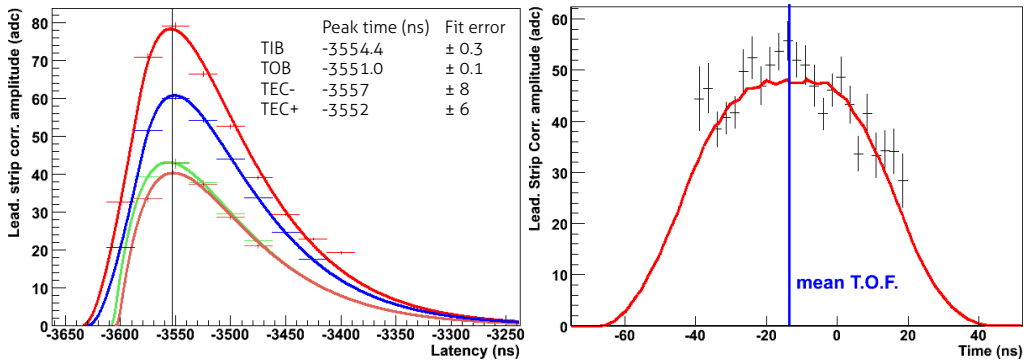

Figure 3: Signal amplitude as a function of trigger timing in a coarse scan (clock cycle) in peak mode (left) and a fine scan ($\sim$1 ns) in deconvolution mode (right).

The last procedure comprises a fine tuning of the synchronization. It involves skewing the clock delay in steps of 1 ns around the expected optimal value for all modules of a given test layer, with the configuration of all other modules in the SST unchanged with respect to the value obtained from the coarse latency scan. Clusters on the test layer compatible with a reconstructed track are used to reconstruct the pulse shape. Figure 3 (right) shows the resulting pulse shape from clusters found in modules of TOB Layer 3, acquired in deconvolution mode. The width of the signal in deconvolution appears broader than in Figure 1 by $\sim$20 ns, due to the jitter of cosmic rays within the 25 ns clock cycle.

3.6 Status of detector operation

At the end of the 2009 commissioning a total 98.1% of the SST was operational. The detailed fractions are summarized in Table 1. The main drops in the operational percentages are the fol-

	Problem			Operational
	Control	Readout	Other	
TIB	1.1%	0.1%	2.3%	96.5 %
TOB	0.9%	0.2%	0.6%	98.3 %
TEC+	0.6%	0.1%	0.5%	98.8 %
TEC-	0.0%	0.1%	0.7%	99.2 %
Total	0.7%	0.2%	1.0%	98.1 %

Table 1: Fraction of problematic and operational readout channels per subdetector and full SST.

lowing: in "TIB control" a loss of 0.98% comes from modules which are kept off, because they are connected to a single cooling loop which was closed in order to reduce the leak of coolant observed. It is foreseen to operate again these modules in the future, when the cooling temperature will be further decreased. In TOB a drop is observed of 0.79% from a single control ring which does not work properly, probably due to a bad electrical connection inside the detector developed after the installation. The fractions named "other" mainly refer to modules which have a broken HV connection, even the modules can be read out properly.

4. Detector performance

In the following sections, the performance of the tracker will be reported using the data collected during CRAFT 2008 and CRAFT 2009, the two main periods of all-CMS data taking when the SST was included, the trigger was setup to detect cosmic rays [19] and the CMS magnet was providing the nominal 3.8 T field. In CRAFT 2008 and 2009 about six and twelve million events where collected respectively.

The event reconstruction and selection, data quality monitoring and data analysis were all performed within the CMS software framework, known as CMSSW [20].

Many detector performance measurements rely either directly or indirectly on the reconstruction of tracks. Two main algorithms were used to reconstruct tracks from cosmic ray muons in CRAFT data: the Combinatorial Track Finder (CTF) and the Cosmic Track Finder. The first is the standard track reconstruction algorithm intended for use with proton-proton collisions, specially re-configured to handle the different topology of cosmic muon events. The second algorithm was devised specifically for the reconstruction of single track cosmic ray muon events. A full description of these algorithms can be found elsewhere [21].

The tracking algorithms use the strip clusters as input. Signal clusters are formed by means of a three threshold algorithm [20]: they are seeded by strips which have a charge that is at least three times above the corresponding channel noise. For each seed, neighboring strips are added if the strip charge is more than twice the strip noise. A cluster is kept if its total charge is more than five times the cluster noise, defined as $\sigma_{\text{cluster}} = \sqrt{\sum_i \sigma_i^2}$, where σ_i is the noise from strip i, and the sum runs over all strips in the cluster.

4.1 Signal cluster charge

The cluster total signal is expected to be proportional to the energy loss in a sensor. In Figure 4

(left) the distribution of signal of clusters associated to a track, corrected for the path length of the particle in the detector is reported. The most probable value of the distributions is the same for the four sub-detectors, as expected, within a few percent.

The signal-to-noise ratio is a benchmark for the performance of the SST. In the signal-to-noise ratio, the cluster noise is divided by $\sqrt{N_{\text{strips}}}$, so that the resulting noise value is approximately equal to the strip noise, independent of the size of the cluster. The cluster charge distributions have

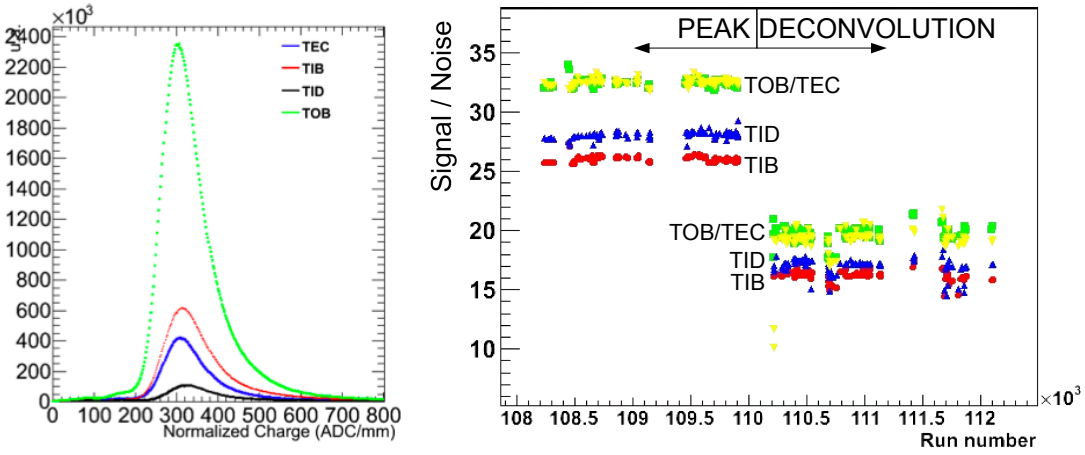

Figure 4: Cluster charge distribution (log scale) and signal-to-noise ratio trend of clusters associated to tracks in all the 4 sub-detectors.

been fitted with a Landau function convoluted with a Gaussian function and the most probable value for the signal-to-noise ratio is shown in Figure 4 (right) as a function of the run number. The result for the peak mode is in the range 27-28 for thin modules and 32-34 for thick ones, compatible with result of CRAFT 2008 [16].

After the switch to deconvolution mode a drop of a factor ~ 1.6 is observed, mainly due to the increased noise, as expected.

4.2 Hit finding efficiency

The hit finding efficiency for a module is measured by extrapolating a track on that module and counting how many times a cluster is found. The results presented here have been determined using the Combinatorial Track Finder, excluding the clusters in the layer of the SST for which the hit efficiency is to be determined. The efficiency results per layer are shown in Fig. 5. The efficiency is higher than 99.5% in all the studied layers, after the bad components are removed. The measured efficiency is the same in runs with the magnetic field off and with the nominal 3.8 T field.

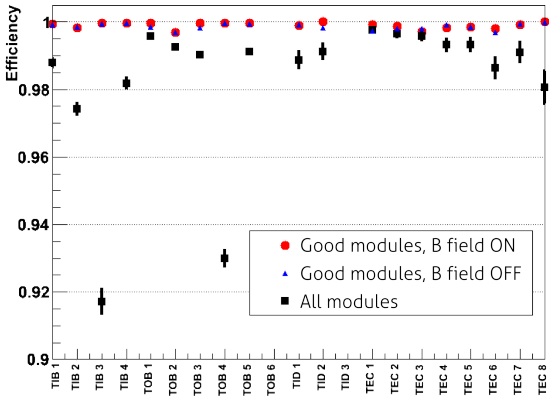

Figure 5: Average module hit efficiency per layer/disk, with and without correction for disconnected or otherwise exclude modules.

4.3 Track finding efficiency

The track reconstruction efficiency is usually measured using an external device to provide a reliable information on the tracks under study. In the case of the SST during the CRAFT 2008, a reference is obtained by requiring the muon chambers to have a track with many hits pointing to the tracker volume. Based on this method, the tracker was reported to have an efficiency between 99.5% and 99.8% [16]. Another method was also used and is briefly described here: the efficiency was measured using data from the tracker only, by reconstructing tracks independently in the upper and lower hemispheres of the tracker.

Tracks in one hemisphere are used as references to measure the efficiency in the other hemisphere. Two such measurements are performed: $\varepsilon(T|B)$, where, given a bottom track, a matching top track is sought and vice versa ($\varepsilon(B|T)$). The matching is performed by requiring that the two opposite-half tracks have pseudorapidities that satisfy $|\Delta\eta| < 0.5$.

The efficiencies measured using this method are shown in Table 2. The efficiencies measured in the Monte Carlo simulation using a realistic detector status are consistent with those measured in the data to within 1% (details of this analysis are given elsewhere [16]).

	combinatorial TF		cosmic TF	
	Data	MC	Data	MC
$\varepsilon(B\|T)$ (%)	97.03±0.07	97.56±0.04	94.01±0.10	93.41±0.06
$\varepsilon(T\|B)$ (%)	95.61±0.08	95.79±0.05	92.65±0.11	93.19±0.07

Table 2: Overall track reconstruction efficiency measured with the top/bottom comparison method.

4.4 Lorentz angle measurement

In the silicon sensors of the barrel, the electric field is perpendicular to the strips. For normal incidence particles, typically only one strip is hit and the cluster size increases with the angle of incidence. In the presence of a magnetic field, however, the drift direction is tilted by the Lorentz angle. This is illustrated, for one module in layer 4 of TOB, in Fig. 6, which shows a profile plot of cluster size versus the tangent of the incidence angle. To extract the Lorentz angle, this distribution is fitted to the function:

$$f(\theta_t) = \frac{h}{P} \cdot p_1 \cdot |\tan\theta_t - p_0| + p_2$$

where h is the detector thickness, P is the pitch, and p_0, p_1 and p_2 are the fit parameters. The parameter p_0 is, in effect, $\tan(\theta_L)$, the value of the minimum of cluster distribution.

The Lorentz angle is measured for each individual module. The mean $\tan(\theta_L)$ is 0.07 ± 0.02 in thin and 0.09 ± 0.01 in thick sensors. The small difference is expected because the hole mobility depends on the electric field (1 and 0.6 V/μm respectively), while the bias voltage applied was uniform (300 V).

The Lorentz angle correction applied to cluster positions during track reconstruction is relatively small – of the order of 10 μm – but it is still larger than the overall alignment precision [22].

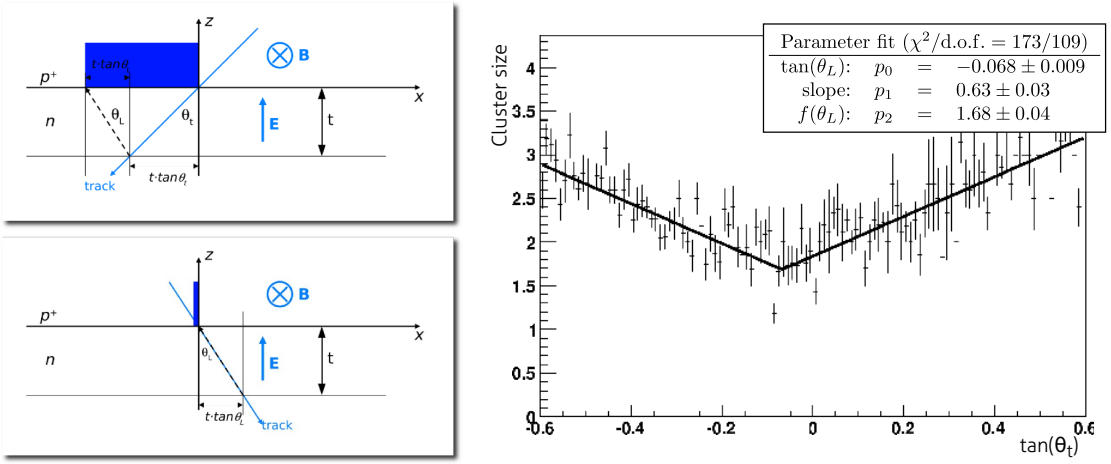

Figure 6: Lorentz drift in the micro-strip sensors. Left: schematic description of the Lorentz angle. Right: Cluster size (in strips) versus incident angle in one module of TOB Layer 4.

5. Conclusions

The CMS Silicon Strip Tracker was fully operated for the first time in 2008, and could be used to make calibration measurements during the CRAFT 2008 data taking, thanks to about 6 millions events containing a track. The SST underwent a major rework of the cooling plant in 2009 and thanks to the experience previously acquired it was re-commissioned in about 5 weeks time between June and July 2009. The following CRAFT 2009 period of data taking provided twelve millions events with cosmic rays in the tracker and saw for the first time the SST in its nominal deconvolution mode.

As much as 98.1% of the detector is operational and the calibrations performed show that nominal performance was obtained in terms of noise, signal, hit finding and tracking efficiencies.

All the commissioning procedures were tested to make sure that the SST is well prepared to the upcoming LHC collisions.

References

[1] CMS Collaboration. The Tracker Project: Technical design report. *CERN-LHCC*, 1998-006, 1998.

[2] J. L. Agram et al. The silicon sensors for the Compact Muon Solenoid tracker – design and qualification procedure. *Nuclear Instruments and Methods in Physics Research Section A: Accelerators, Spectrometers, Detectors and Associated Equipment*, 517(1-3):77 – 93, 2004.

[3] CMS Collaboration. The CMS Cosmic Run at Four Tesla. arXiv:0911.4845, to be published on JINST.

[4] M. Raymond et al. The CMS Tracker APV25 0.25 μm CMOS Readout Chip. *Proceedings of the 6th workshop on electronics for LHC experiments, Krakow*, page 130, 2000.

[5] J. Troska et al. Optical readout and control systems for the CMS tracker. *IEEE Trans. Nucl. Sci.*, 50:1067–1072, 2003.

[6] C. Foudas et al. The CMS tracker readout front end driver. *IEEE Trans. Nucl. Sci.*, 52:2836–2840, 2005.

[7] F. Drouhin et al. The CERN CMS tracker control system . *Nuclear Science Symposium Conference Record, IEEE*, 2:1196, 2004.

[8] Kostas Kloukinas et al. FEC-CCS: A common front-end controller card for the CMS detector electronics. *Proceedings of the 12th Workshop on Electronics for LHC and Future Experiments (LECC 2006), Valencia*, page 179, 2006.

[9] C. Paillard, C. Ljuslin, and A. Marchioro. The CCU25: A network oriented communication and control unit integrated circuit in a 0.25-mu-m CMOS technology. *Proceedings of the 8th Workshop on Electronics for LHC Experiments, Colmar*, page 174, 2002.

[10] S. Gadomski et al. The Deconvolution method of fast pulse shaping at hadron colliders. *Nucl. Instrum. Meth.*, A320:217–227, 1992.

[11] G. Cervelli, A. Marchioro, P. Moreira, and F. Vasey. A radiation tolerant laser driver array for optical transmission in the LHC experiments. *Proceedings of the 7th Workshop on Electronics for LHC Experiments, Stockholm*, 2001.

[12] CMS Collaboration. CMS trigger and data-acquisition project: Technical design report, Volume 2: Data-acquisition and high-level trigger. *CERN-LHCC*, 2002-026, 2002.

[13] P. Placidi, A. Marchioro, P. Moreira, and K. Kloukinas. A 40-MHz clock and trigger recovery circuit for the CMS tracker fabricated in a 0.25-mu-m CMOS technology and using a self calibration technique. *Proceedings of the 5th Workshop on Electronics for the LHC Experiments, Snowmass, Colorado*, page 469, 1999.

[14] D Ricci, L Amaral, S Dris, K Grill, A Jimenez Pacheco, F Palmonari, V Radicci, A V Singovsky, J Troska, and F Vasey. CMS Tracker, ECAL and Pixel Optical Cabling: Installation and Performance Verification. *Proceedings of Topical Workshop on Electronics for Particle Physics TWEPP-07, Naxos, September 2008*, pages 477–482, 2008.

[15] W. Adam et al. Performance studies of the CMS Strip Tracker before installation. *JINST*, 4:P06009, 2009.

[16] CMS Collaboration. Commissioning and Performance of the CMS Silicon Strip Tracker with Cosmic Ray Muons, 2009.

[17] CMS Collaboration. Performance of the CMS Drift-Tube Local Trigger with Cosmic Rays. arXiv:0911.4893, to be published on JINST.

[18] C. Delaere et al. Procedure for the fine delay adjustment of the CMS tracker. *CMS Note*, 2008/007, 2008.

[19] CMS Collaboration. Performance of the CMS Level-1 Trigger during Commissioning with Cosmic Rays. arXiv:0911.5422, to be published on JINST.

[20] CMS Collaboration. CMS physics: Technical design report. *CERN-LHCC*, 2006-001, 2006.

[21] W. Adam et al. Stand-alone Cosmic Muon Reconstruction Before Installation of the CMS Silicon Strip Tracker. *JINST*, 4:P05004, 2009.

[22] CMS Collaboration. Alignment of the CMS inner tracking system with cosmic ray particles. arXiv:0910.2505, to be published on JINST.